PERGAMON

International Journal of Heat and Mass Transfer 44 (2001) 843–855

International Journal of HEAT and MASS TRANSFER

www.elsevier.com/locate/ijhmt

Transient cooling effect by wall mass injection after backstep in high temperature flow field

Jing-Tang Yang*, Jing-Der Gu, Wan-June Ma

Department of Power Mechanical Engineering, National Tsing Hua University, Hsinchu 30043, Taiwan

Received 2 March 2000

Abstract

A new experimental methodology was developed to study the transient mixing process of the high temperature flow field behind the backstep with low temperature fluid injected from the lower surface. Temporal data show that the flow temperature at locations between 0.2 and 0.4 reattachment lengths, Xr, at 1-mm height dropped faster than other places. Temporal temperature difference across the wall plate performed quite different trends before and after 0.6 time the reattachment length. The temporal Nusselt number distribution over the entire wall plate reached its peak value about 5–10 s after the wall injection initiated and gradually converged to a steady-state value. © 2001 Published by Elsevier Science Ltd.

Keywords: Transient cooling; Wall mass injection; Backstep mixing; Experimental methodology and results

1. Introduction

The transient process of high temperature flow field behind the backstep with low temperature fluid injected from the lower surface was studied experimentally. As shown in Fig. 1, flow field separates at the tip of the step and reattaches the lower surface at the reattachment point. The flow within the recirculating zone after the step consists of a pair of vortex. The recirculating vortex causes a leftward flow near the surface and separates again around the corner of the step. The secondary separation induces the corner eddy. The large velocity between the free stream and the recirculating zone generates a shear layer with high turbulent energy.

The basic backstep flow field has been studied for over a half of the century. Many researchers paid their attention to the size of the recirculating zone. Eaton and Johnston [1] concluded that the reattachment length was influenced by several factors: the turbulence intensity, the boundary layer status of inlet flow, the aspect ratio of the test section, and the pressure gradient of the flow field etc. de Brederode and Bradshaw [2] showed that the three-dimensional features could be neglected if the aspect ratio of the step was greater than 10. Richardson et al. [3] reported that the size of the recirculating zone and the intensity of the recirculating flow were reduced by the injected flow. The wall-injection flow also reduced the recirculating velocity in the recirculating zone. Yang et al. [4] found the velocity fluctuation and Reynolds stress of the flow field decreased by increasing the wall-injection flow rates. Yogesh and Raghunandan [5] injected both fuel and nitrogen to investigate the heat transfer behavior of the bottom plate. Zvulouni et al. [6] studied, on the

* Corresponding author. Tel.: +886-3-5715131, ext. 3773; fax: +886-3-5722840/5726846.

E-mail address: jtyang@pme.nthu.edu.tw (J.T. Yang).

0017-9310/01/$ - see front matter © 2001 Published by Elsevier Science Ltd.
PII: S0017-9310(00)00130-7

Nomenclature

U	mean velocity	Xr	reattachment length
u	velocity fluctuation	Nu	Nusselt number
T	mean temperature	k	thermal conductivity
Re	Reynolds number	t	thickness of porous plate
V_w	superficial velocity of injected air		
Q_w	volumetric flow rate of injected air	*Greek symbols*	
A_p	area of porous plate	Φ	porosity of porous plate
TI	turbulence intensity	δ^*	displacement thickness of boundary layer
H^*	shape factor	θ	momentum thickness of boundary layer

basis of a dump combustor model instead of mass-injected plate, the heat transfer performance of high temperature flow field with wall injection. Yang and Tsai [7] experimentally investigated the characteristics of heat transfer in a steady separated flow field with cool-air injection and concluded that the maximum heat flux appeared near the reattachment point. Yang et al. [8] considered to be a combustor model with PMMA vapor pyrolyzed from the lower surface after the step and found that the flow field showed different transient ignition processes depending on either flow mixing or temperature characteristics near the wall. Martin et al. [9] placed porous inserts after the step to change the size and heat transfer characteristics of recirculating zone successfully.

The researches mentioned above are mostly limited to the steady state flow field or heat transfer phenomena. The transient features need further study to clarify. Thus, the present study concentrated on the transient cooling period between the beginning of the low temperature wall injection and the time the steady flow developed. As a result, a reliable methodology for studying the transient cooling effect was successfully established and the temporal temperature data was recorded and systematically studied.

2. Experimental design

2.1. Test facilities

A test section was constructed, as shown in Fig. 2, to establish the high temperature flow field. The width of the test section was 200 mm, the inlet channel height was 30 mm and the step height was 15 mm. A porous plate made of stainless steel was placed just behind the backstep. The average pore size of the plate was 10 μm and the overall porosity was 40.8%. High-pressure air was pumped into a settling tank beneath the test section and flew through porous wall to form a wall-injection flow. A heat exchanger was placed between the porous plate and the air tank, through which the cold water stream was used to keep the wall-injection air at the specified low temperature.

High temperature air was used as working fluid and was supplied by a wind tunnel system, as shown in Fig. 3. The main airflow stream was provided with a 76 kW blower and a frequency inverter. A vitiator burning liquefied petroleum gas (LPG) was built to heat the main air stream. Before entering the test section, the air stream passed through a divergent section, a settling chamber and a convergent section. The con-

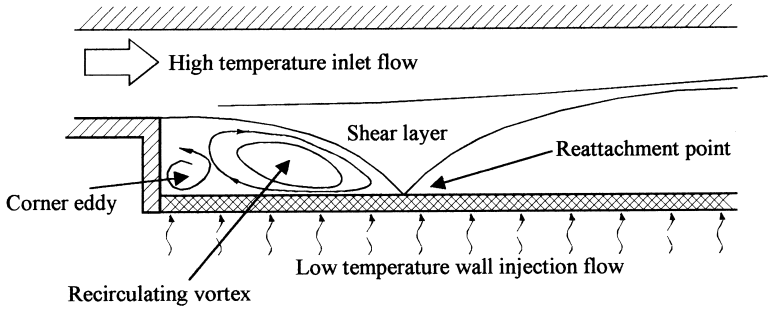

Fig. 1. Schematic diagram of the backstep flow field with base mass injection.

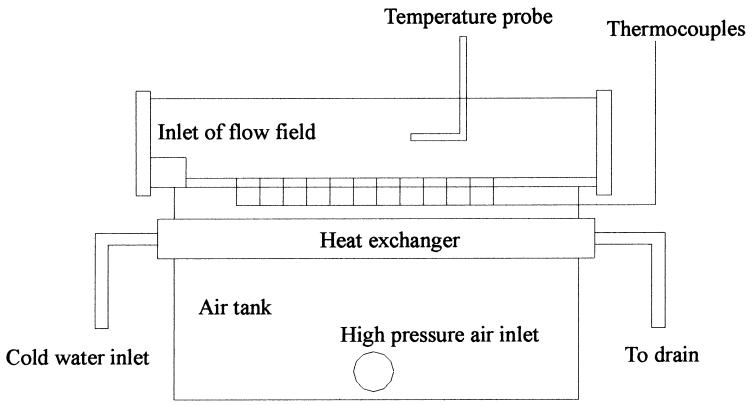

Fig. 2. Schematic diagram of the test section.

traction ratio of the convergent section was 40 and a layer of honeycomb made of steel was placed inside the settling chamber to reduce the turbulence intensity of the inlet flow.

The flow features were measured by the TSI two-component forward-scattered laser-Doppler velocimetry. A coherent 5-W argon-ion laser was used as laser beam source and aluminum oxide (Al_2O_3) powders with average particle size 1 μm were used as seeding particles. Scattered laser signals were received and processed by a set of optical receivers, signal processors and digital counters. The temperature measurement system consisted of two parts: the wall temperature was measured by Omega 125-μm thermocouples buried inside the porous plate, and the flow temperature was measured by a thermocouple probe containing 25-μm K-type thermocouple wires. The temperature signals were processed by a charge amplifier and A/D interface cards and was recorded onto PC diskettes. The transient process was defined as the period from the wall-injection flow entered the flow field till the mixing flow field approached a new steady state. The temporal starting point of this process was chosen as the temperature signals at the lower surface of the porous plate began to drop. The sampling rate of the temperature signal was 50 Hz. An un-weighted, moving-window averaging scheme was used to smooth the data. The window width was chosen as 0.4 s.

2.2. Uncertainty analysis

The air entering the test section was not pure air

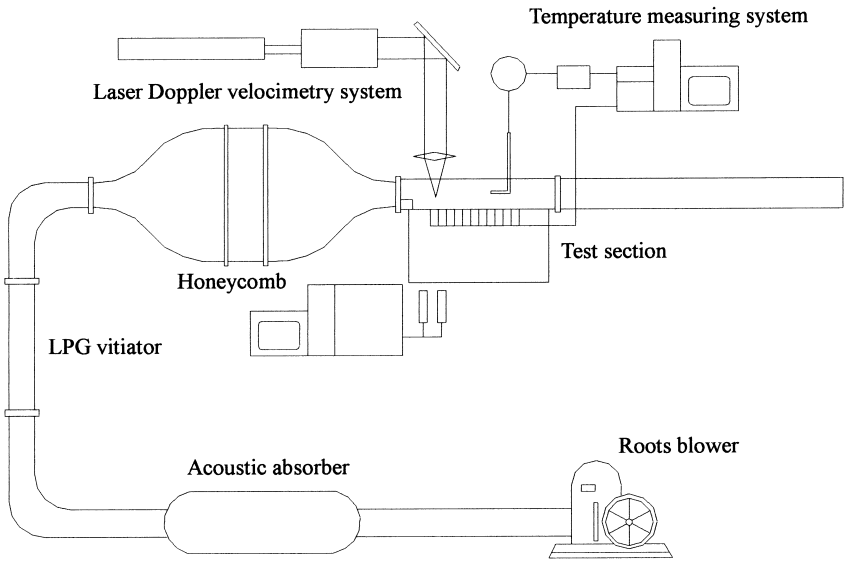

Fig. 3. Schematic diagram of the wind tunnel system.

because it was blended with the combustion products in the LPG vitiator. However, the overall fuel/air ratio in the vitiator was less than 0.01, and thus it was reasonable to treat the working fluid as standard air. To ensure the two-dimensionality of the flow field, the aspect ratio of the test section must be greater than 10 [2]. The aspect ratio was 13.3 and certainly fit the requirement. Furthermore, the velocity field measurements were conducted along the center plane of the test section and confirmed the two-dimensionality.

On the whole, the position of maximum uncertainty of the flow field was located at the shear layer. After repetitive measurements in the shear layer 10-mm downstream of the tip of the step, based on 95% confidence level, the estimated maximum uncertainty of mean velocity was 4.3%. The corresponding uncertainties in turbulent intensity, Reynolds stress and flow field temperature were 4.9, 4.5 and 2.0%, respectively. After 1024 repetitive measurements at the same measuring point, the maximum uncertainty of wall temperature was estimated as 2.5%.

2.3. Test conditions

The temperature and velocity in the free stream 2-cm upstream the step were 200°C and 20 m/s, respectively. The Reynolds number defined by Eq. (1) was 9085.

$$Re_h = \frac{U_0 H}{\nu} \tag{1}$$

where U_0, H and ν were inlet velocity, step height and kinematics viscosity, respectively.

The superficial velocity of the wall-injection flow was 0.24 m/s, relative to a volume flow rate of 0.35 m^3/min. Mean superficial velocity was defined as

$$V_w = \frac{Q_w}{\Phi A_p} \tag{2}$$

where Q_w, Φ and A_p were wall-injection rate, porosity, and porous plate area, respectively.

3. Results and discussion

3.1. Inlet conditions

According to Eaton and Johnston [1], the inlet condition significantly affected the flow field. It was thus necessary to examine the inlet flow conditions before any further discussion was proceeded. The boundary layer properties of the inlet condition were listed in Table 1. The measuring cross section was located at 20 mm upstream of the step. The boundary layer thickness δ was based on the 99% of maximum local velocity and the displacement thickness δ^*, momentum thickness θ, shape factor H^* and turbulence intensity TI were defined, respectively, as follows:

$$\delta^* = \int_0^\infty \left(1 - \frac{U}{U_{max}}\right) dy \tag{3}$$

$$\theta = \int_0^\infty \frac{U}{U_{max}} \left(1 - \frac{U}{U_{max}}\right) dy \tag{4}$$

$$H^* = \frac{\delta^*}{\theta} \tag{5}$$

$$\mathrm{TI} = \frac{1}{U_0} \sqrt{\frac{\overline{u^2} + \overline{v^2}}{2}} \tag{6}$$

where U, U_{max} and u denoted the local mean velocity, the maximum velocity of the cross section, and the local velocity fluctuation.

According to Pitz and Daily [10], the shape factor for turbulent flow was less than 1.3. The shape factor of present study was 1.11, which meant that the inlet flow was in turbulent regime. Furthermore, the average turbulence intensity in the boundary layer was 8.0%, exceeding the laminar flow limit 5% (accepted in general), and, hence, the flow field of present research should be in turbulence regime.

3.2. Mean velocity distribution

The momentum of the wall-injection flow was much smaller than that of the main stream. This low-energy

Table 1
Inlet condition

Inlet temperature (°C) and velocity (m/s)	Reynolds number (Re_h)	Boundary layer thickness δ (mm)	Momentum thickness θ (mm)	Shape factor (H^*)	Turbulence intensity, TI (%)	
					Free stream	Boundary layer
200 and 20	9085	7.2	0.44	1.11	4.1	8.0

fluid stream would slow down the main stream in near wall region. But the main stream did not contact directly with the wall-injection fluid in the upper half of the flow field. On the contrary, based on continuity equation, the flow velocity was accelerated by adding extra mass into the flow field. These two opposite tendencies can be observed in Fig. 4. The mean velocity distribution in horizontal direction decreased when wall-injection rate increased in near wall region. On the other hand, the mean horizontal velocity in upper region increased when wall-injection rate increased.

The mean velocity in vertical direction was strongly influenced by the main recirculating eddy. This stationary vortex rotated clockwise, as illustrated in Fig. 1. In other words, the flow direction on right half of the vortex was downward and the flow direction on left half of the vortex was upward. Because the wall-injection flow was upward, the vertical velocity of the flow field, especially in near wall region, was accelerated on left half of the main vortex and decelerated on right half of the main vortex, as depicted in Fig. 5. The mean velocity distribution in vertical direction increased when wall-injection rate increased before 60% reattachment length. The mean vertical velocity in vicinity of the wall after the recirculating zone decreased when wall-injection rate increased.

3.3. Turbulence phenomena

The measured distribution of turbulence intensity is shown in Fig. 6. Since the porous plate screened the wall-injected fluid and the superficial velocity of the

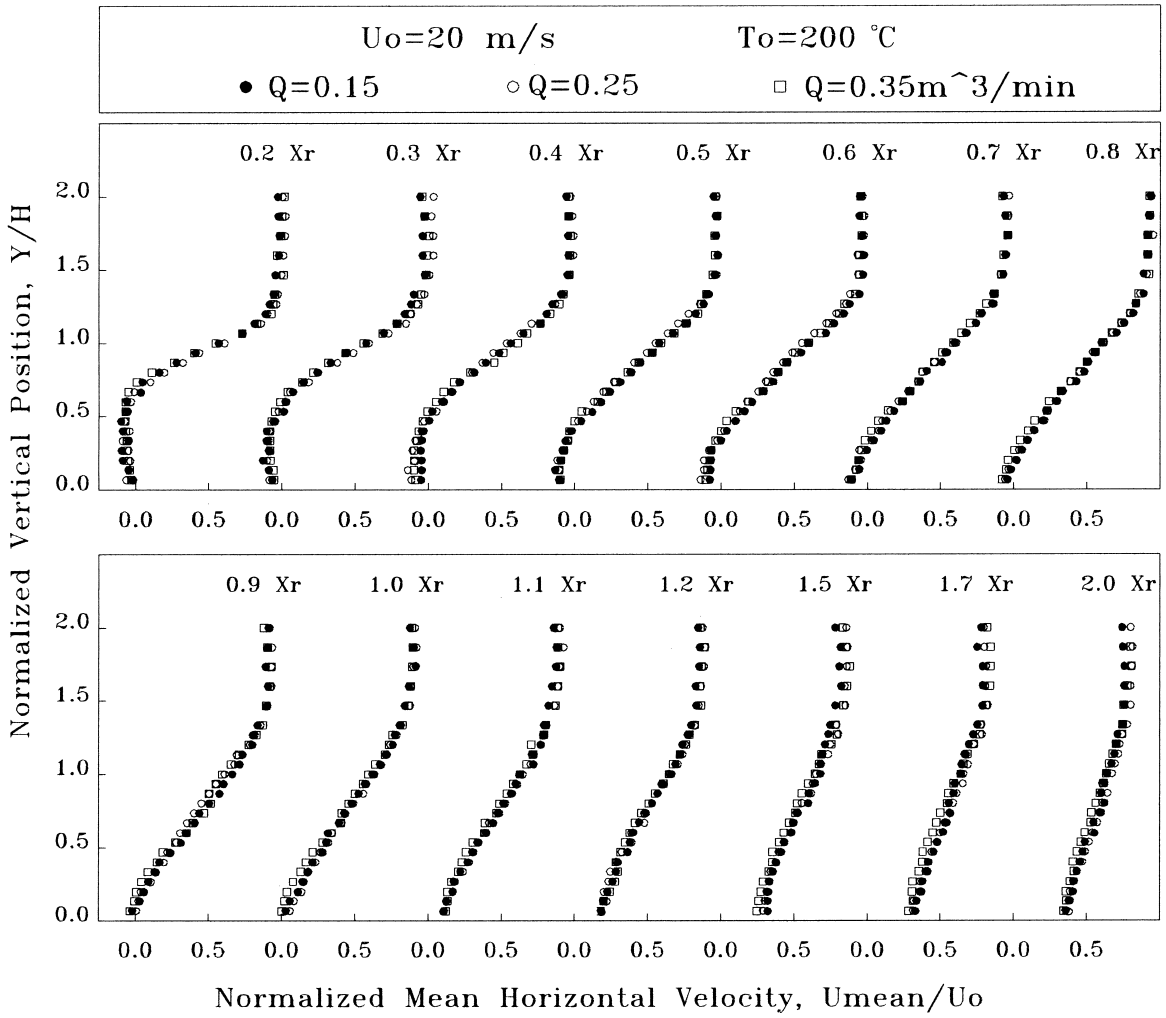

Fig. 4. Mean horizontal velocity distribution of different wall-injection flow rates ($T_0 = 200°C$; $U_0 = 20$ m/s; Q = 0.15, 0.25, 0.35 m^3/min).

fluid was very low, the injection flow possessed relative lower turbulence intensity. After this low turbulence fluid stream entered the flow field, the turbulence strength of the flow field below shear layer was reduced immediately. As the flow velocity in the upper half of the flow field was increased by wall-injected flow and the wall-injected fluid with low turbulence intensity could not reach this region directly, the turbulence intensity in this region was enhanced.

The Reynolds stress distribution shown in Fig. 7 indicates that the turbulence was produced mainly in shear layer. The shear layer contained the greatest velocity gradient of the flow field and hence had the largest Reynolds stress. The Reynolds stress below the shear layer was obviously reduced by the wall-injection flow before the reattachment point. After the reattachment point, the low-turbulence injected flow was restricted near the wall due to the lack of recirculating structure, and consequently reduced the local Reynolds stress.

3.4. Temporal variation of flow field temperature

The temporal variation of flow field temperature from 0 to 80 s is shown in Fig. 8. When $t = 0$, i.e. just before the wall-injection flow entered the flow field, the temperature distribution was homogeneous. At $t = 3$ s, the low temperature fluid gathered around the step corner. Because the recirculating vortex rotated clockwisely, the low temperature fluid injected from the wall was swept toward left near the wall. The accumulation effect of the low temperature fluid lowered the temperature in this area quickly. The complicated temperature contours on right half of the recirculating

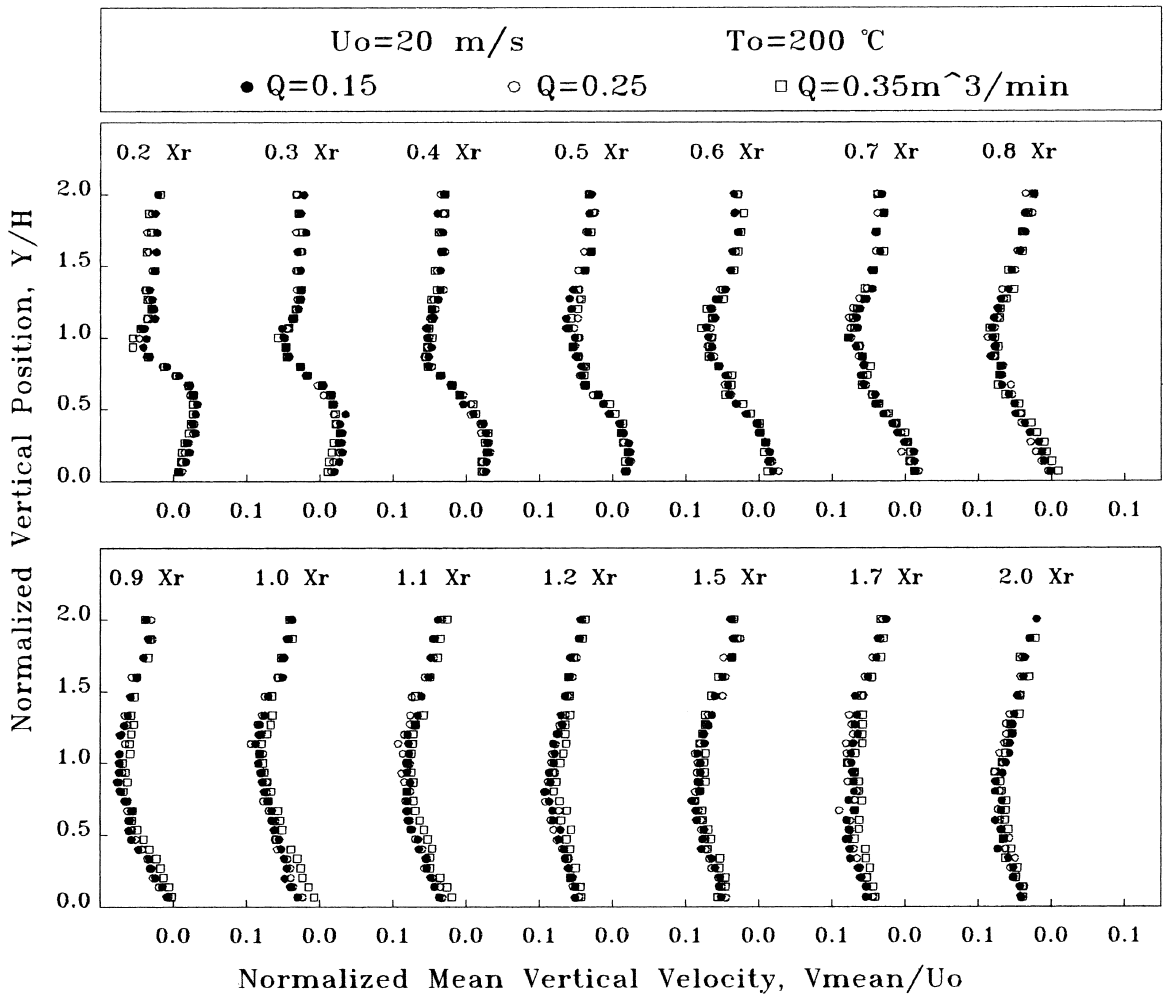

Fig. 5. Mean vertical velocity distribution of different wall-injection flow rates ($T_0 = 200$°C; $U_0 = 20$ m/s; $Q = 0.15, 0.25, 0.35$ m^3/min).

zone meant considerable-mixing processes happened there. At $t = 15$ s, the low temperature fluid continued to accumulate around the step corner. The size of the low temperature region at the corner of the step expanded and formed a triangle shape. The temperature contours on downstream side became more and more smooth. Finally, at $t = 80$ s, the low temperature triangle fixed its shape and size at the step corner. Its bottom width was about 0.6 times of the reattachment length. In near wall region, this low temperature region might extend toward the reattachment point. Most of the low temperature fluid was pushed toward the step corner after leaving the porous plate. The temperature contours on downstream side were relatively steady and smooth.

Fig. 9 shows the temporal variation of the flow temperature at 1-mm height above the base. The horizontal distance was normalized by the reattachment length, Xr. At the beginning of the injection, the temperature of the flow between locations 0.2 and 0.4Xr dropped faster than in other places. This phenomenon was consistent with the temporal temperature distribution, as shown in Fig. 8. At the time near the fully developed stage, the temperature separated into two groups. Locations before 0.6Xr showed obvious lower temperature than that after 0.6Xr. The low temperature zone before 0.6Xr was inside the triangle low temperature area as depicted in Fig. 8. Fig. 10 indicates that the locations before 0.4Xr at 6-mm height still showed rapid temperature reduction at the beginning of injection. But the reducing trend was not so tense as that at 1-mm height. At steady state stage, the limit of low temperature area was shortened from 0.6Xr as in 1-mm height case to the region from 0.2 to 0.4Xr. It

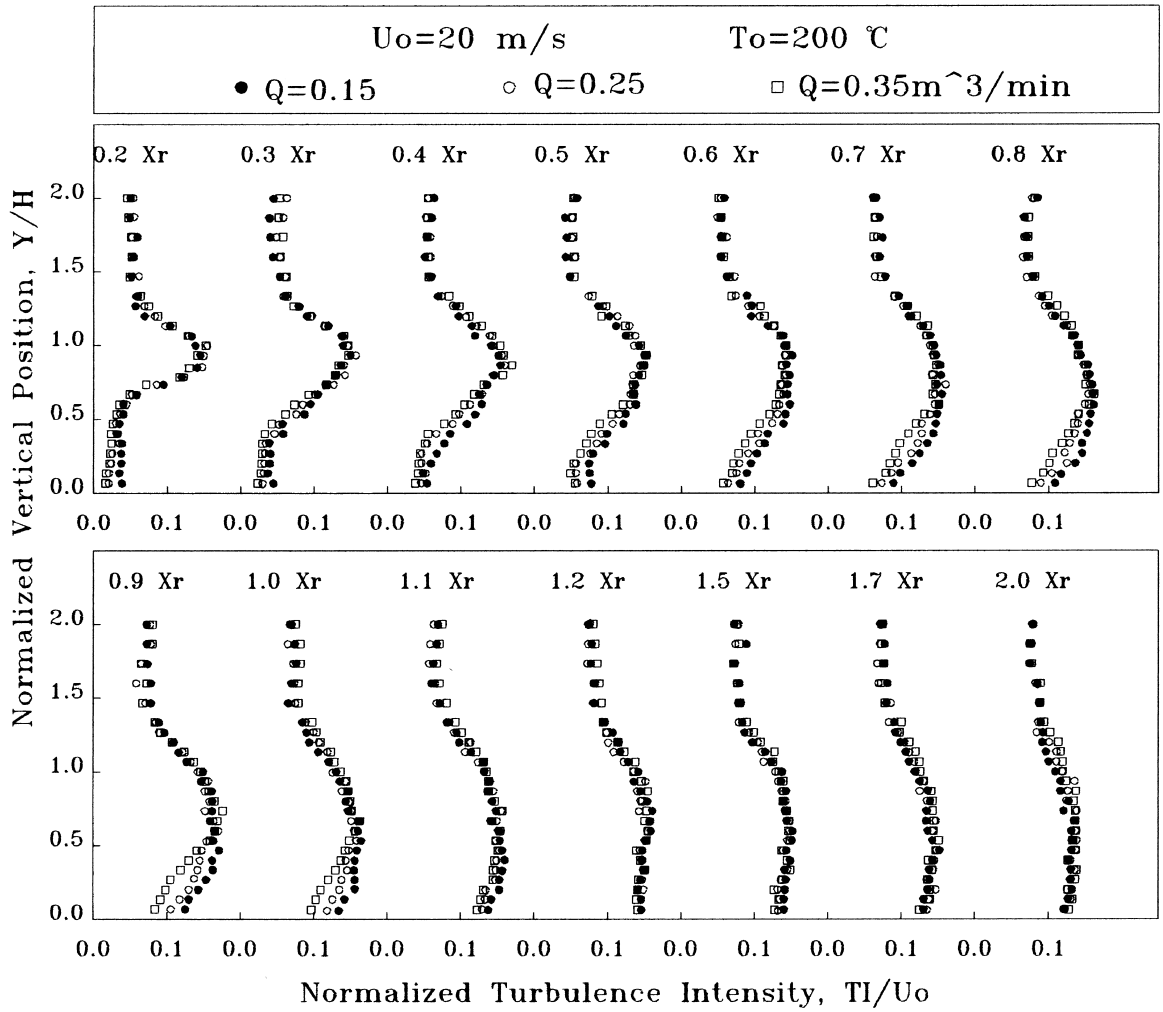

Fig. 6. Turbulence intensity distribution of different wall-injection flow rates ($T_0 = 200$°C; $U_0 = 20$ m/s; Q = 0.15, 0.25, 0.35 m^3/min).

still matched the shape of low temperature triangle. The temporal variation of flow field temperature at 12-mm height is shown in Fig. 11. The temperature variation history was quite different from that of 1-mm height. At 12-mm height, the low-temperature-triangle near the corner covered very small portion in horizontal direction. That is, in Fig. 10, only 0.2Xr location showed a more rapid temperature drop than elsewhere. At the locations from 0.4 to 0.2Xr, flow field temperatures were not obviously influenced by the wall-injection fluid.

Fig. 12 shows a temporal temperature distribution in horizontal direction at 1-mm height. After the low temperature fluid injected into the flow field, the temperature near the corner dropped quickly especially at location 0.4Xr. After 50 s, the horizontal temperature distribution came into steady state except the very near corner location 0.2Xr, where the temperature came into steady state until 120 s after injection. Fig. 13 shows the temporal temperature distribution in horizontal direction at 12-mm height. The flow temperature was not reduced so much as that at 1-mm height. But there still existed a quick-drop area near the corner zone. It was reasonable to interpret this by the influence of low temperature triangle mentioned before.

3.5. Wall heat transfer

The wall heat transfer effect was evaluated by Nusselt number, which was calculated on the basis of free stream temperature and the temperature difference of both sides of the porous wall, as follows:

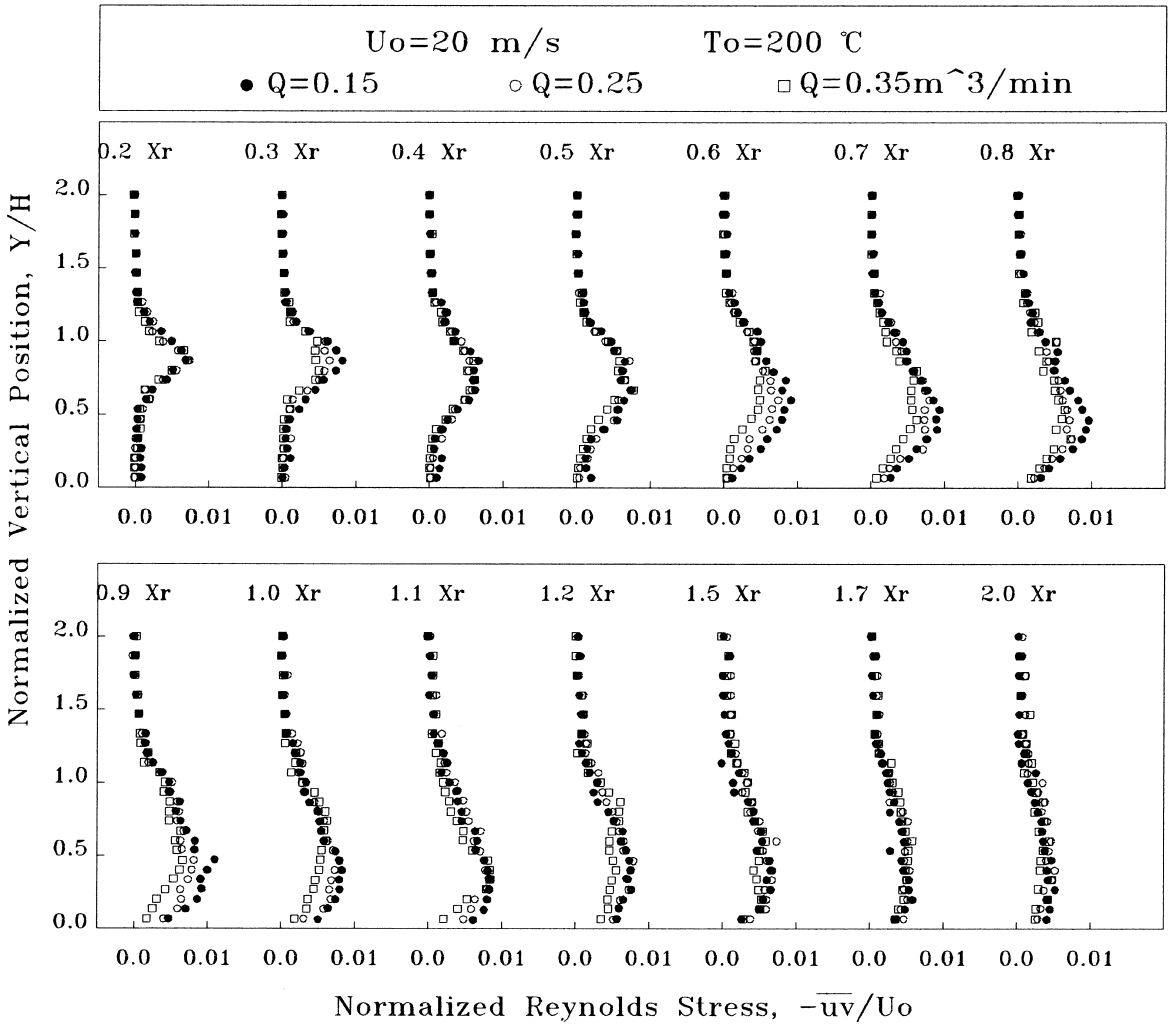

Fig. 7. Reynolds stress distribution of different wall-injection flow rates ($T_0 = 200°C$; $U_0 = 20$ m/s; Q = 0.15, 0.25, 0.35 m^3/min).

$$Nu = \frac{\Delta T\, H k_p}{(T_u - T_0) t k_f} \tag{7}$$

where

$$k_p = \Phi k_f + (1 - \Phi) k_s \tag{8}$$

k_p, k_f and k_s denoted thermal conductivity of working fluid stainless steel, and porous material, respectively. T_0, T_u and ΔT denoted, respectively, the inlet temperature, the temperature on upper surface of porous plate, the temperature difference of both sides of the porous wall, and t denoted the thickness of porous plate.

Fig. 14 shows the temporal temperature difference between both sides of porous wall, ΔT, at different horizontal locations. The temperature difference inside recirculating zone between 0.2 and 0.6Xr began to drop about 10 s after the wall injection started. The locations outside the recirculating zone (1.0 or 1.3Xr), however, did not follow this trend. After low temperature flow injected the temperature on the lower surface of the porous plate dropped faster than that on the upper surface and caused the temperature difference to increase. After some time (for example, 10 s), the low temperature fluid accumulated inside the recirculating zone and caused the flow field temperature to be relatively lower than elsewhere. Since the temperature on the upper surface of the porous plate inside the recirculating zone was low, the temperature difference in this area thus dropped.

Fig. 15 shows the temporal variation of Nusselt number. The Nusselt number reached its maximum value near the reattachment point and this trend was consistent with the conclusion of Yang and Tsai [8]. On the contrary, the Nusselt number was relatively

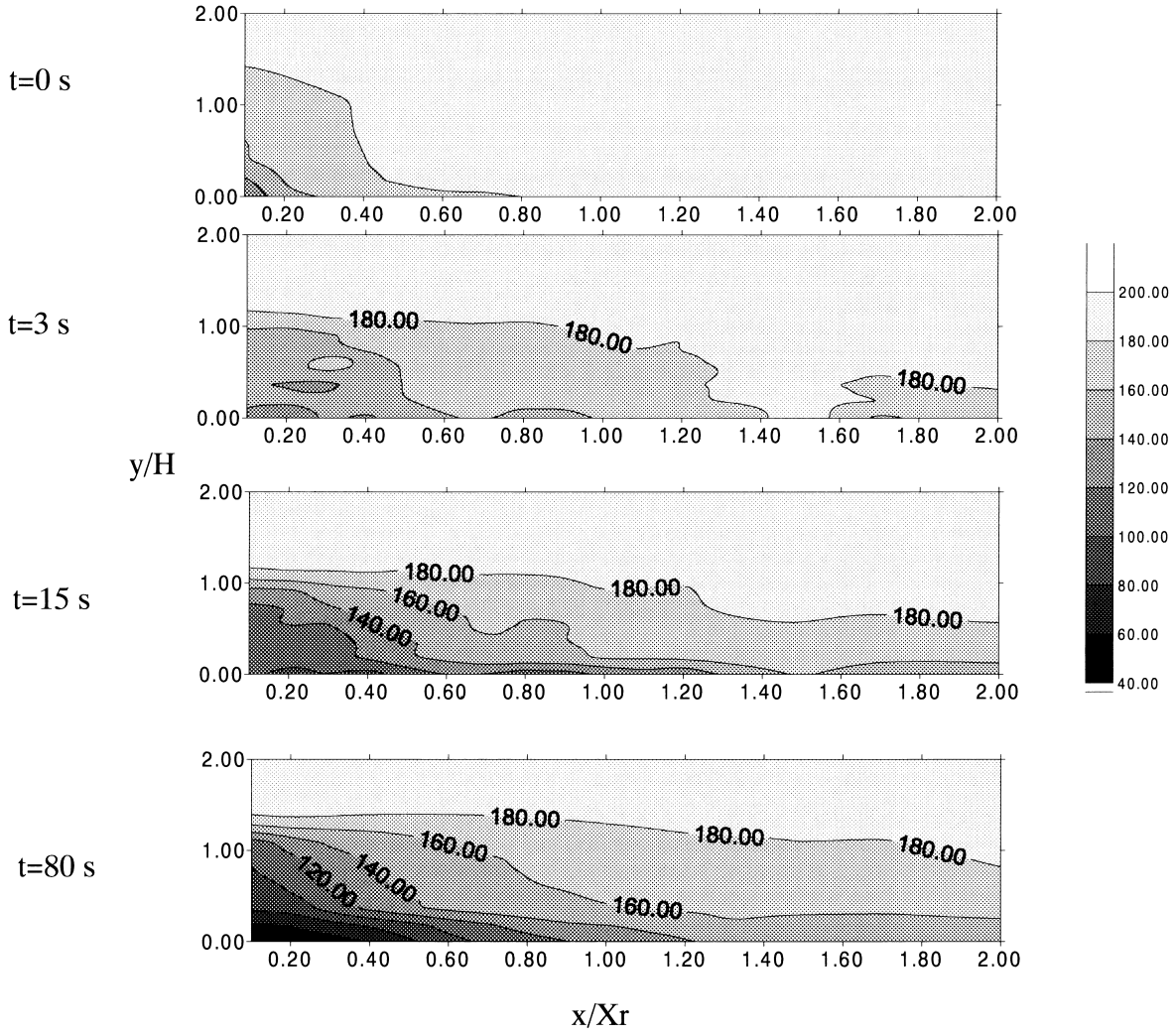

Fig. 8. Temporal variation of flow field temperature distribution ($T_0 = 200$°C; $U_0 = 20$ m/s; $Q = 0.35$ m^3/min).

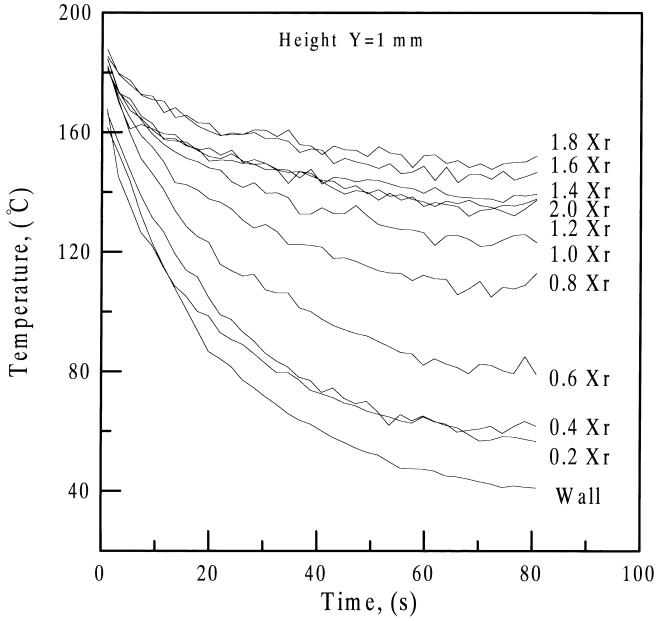

Fig. 9. Temporal variation of flow field temperature distribution at 1-mm height ($T_0 = 200°C$; $U_0 = 20$ m/s; $Q = 0.35$ m^3/min).

low near the step. The heat convection at this region was not so lively due to the existence of low temperature zone near the corner. No matter what locations in horizontal direction, the Nusselt number reached its peak value nearly 5–10 s after the wall injection initiated and converged to a steady-state value.

4. Conclusions

An experimental methodology was developed to study the transient process of high temperature flow field behind the backstep mixing with the low temperature fluid injected from the lower surface. The experimental results can be described as follows:

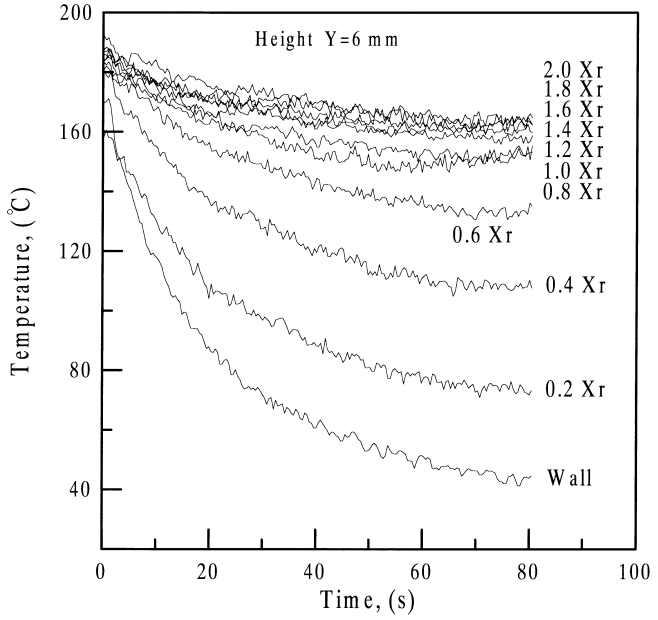

Fig. 10. Temporal variation of flow field temperature distribution at 16-mm height ($T_0 = 200°C$; $U_0 = 20$ m/s; $Q = 0.35$ m^3/min).

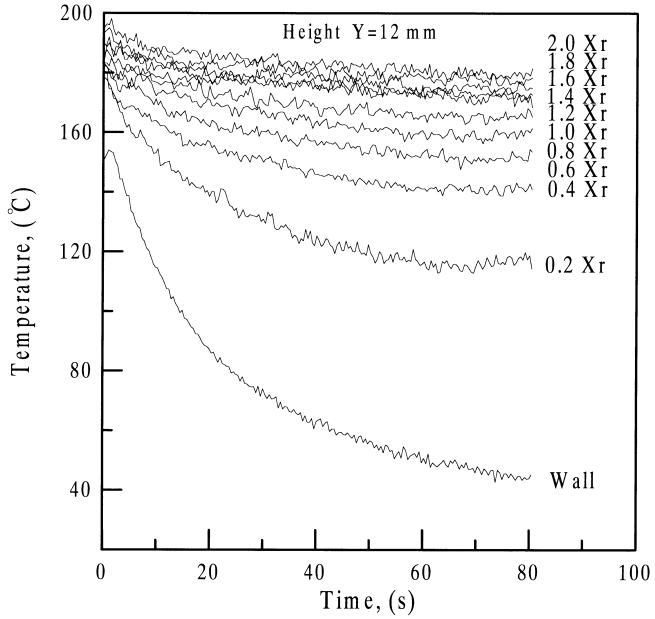

Fig. 11. Temporal variation of flow field temperature distribution at 12-mm height ($T_0 = 200°C$; $U_0 = 20$ m/s; $Q = 0.35$ m^3/min).

As the wall-injection rate increased, the mean horizontal velocity of the flow decreased in near-wall region and increased in the free stream. The mean vertical velocity before 60% reattachment length increased by the existence of wall-injection flow and decreased in the near-wall zone after 60% reattachment length. When wall-injected fluid entered the flow field, both the turbulence strength and Reynolds stress of the flow field below shear layer was reduced whereas they increased in the region above the shear layer. Down-

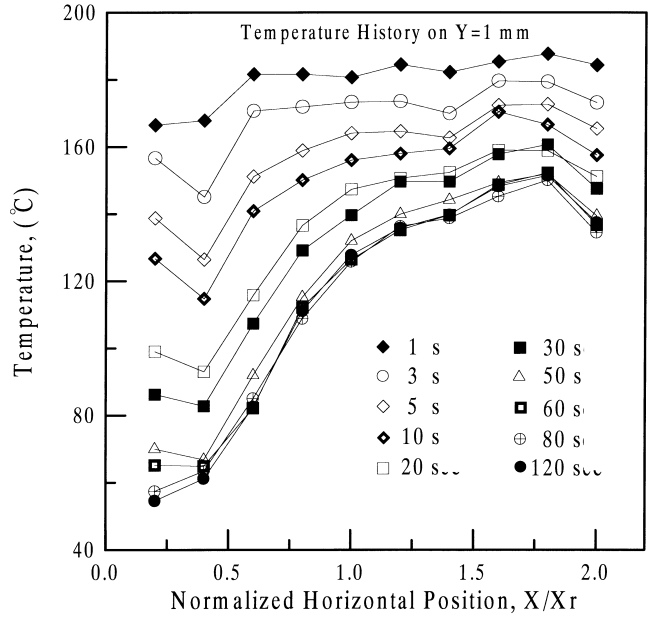

Fig. 12. Temporal variation of flow field temperature distribution near the wall ($T_0 = 200°C$; $U_0 = 20$ m/s; $Q = 0.35$ m^3/min; height, 1 mm).

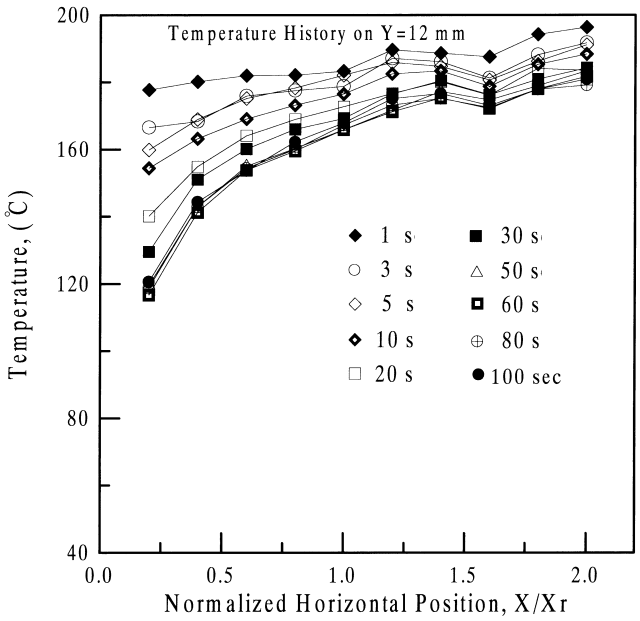

Fig. 13. Temporal variation of flow field temperature distribution near the wall ($T_0 = 200°C$; $U_0 = 20$ m/s; $Q = 0.35$ m^3/min; height, 12 mm).

stream of the recirculating region, the low-turbulence injected flow was confined near the wall, and thus, reduced the local Reynolds stress.

At the beginning of the injection cooling, the low temperature fluid accumulated near the wall region around the step corner. The size of the low temperature region at the corner then gradually expanded to form a triangle shape, of which bottom width was about 0.6Xr. Temporal data show that the flow temperature at locations between 0.2 and 0.4Xr at 1-mm height dropped faster than other places once the low temperature fluid started to inject, and, then, the temperature curves separated into two groups: locations before 0.6Xr had obvious lower temperature than those after 0.6Xr. At a higher section of 6-mm height, the region before 0.4Xr still showed rapid temperature reduction at the beginning of injection, whereas the decreasing trend was not so profound as compared with that of 1-mm height. In addition, the flow temperature near the wall around the corner dropped

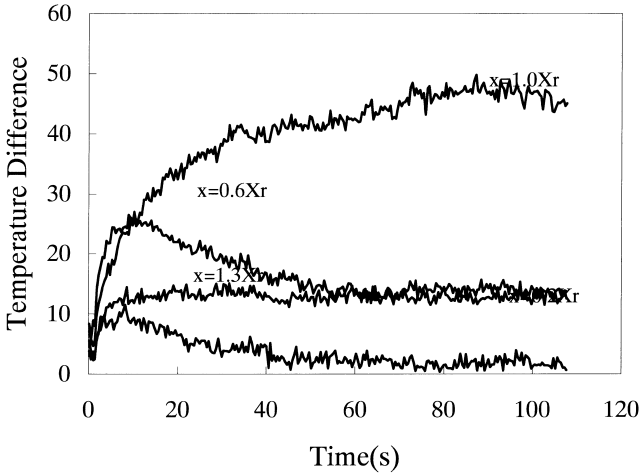

Fig. 14. Temporal variation of temperature difference between both sides of porous plate ($T_0 = 200°C$; $U_0 = 20$ m/s; $Q = 0.35$ m^3/min; $x = 0.2$, 0.6, 1.0, 1.3Xr).

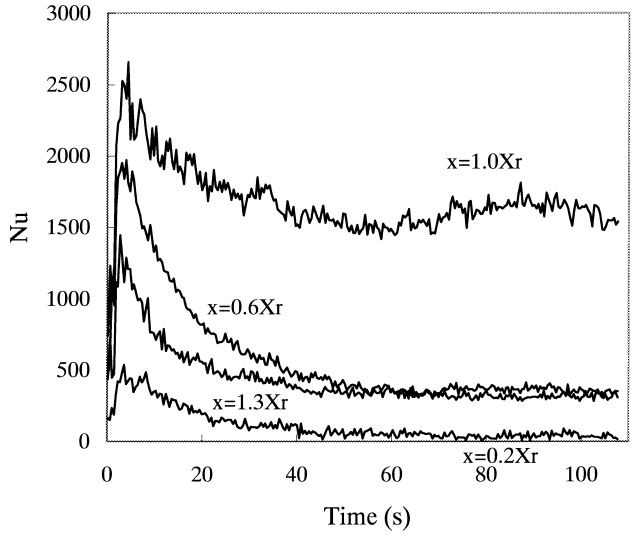

Fig. 15. Temporal variation of Nusselt number at different location of the wall ($T_0 = 200°C$; $U_0 = 20$ m/s; $Q = 0.35$ m^3/min; $x = 0.2, 0.6, 1.0, 1.3$Xr).

steeply especially at location 0.4Xr. After 50 s, the horizontal temperature distribution came into a steady state except the very near corner location. The flow temperature at this location came into a steady state until 120 s after injection.

The temperature difference across the wall plate before 0.6Xr rose considerably at the beginning and began to drop 10 s after wall injection whereas that in downstream increased monotonously with time. The temperature difference in the redeveloping boundary layer also increased with time, but reached a steady state within a much shorter time. The corresponding Nusselt number reached its maximum value near the reattachment point while that was relatively low near the step corner. The trend revealed that the existence of the low temperature zone near the corner subdued the heat convection at that area. The temporal Nusselt number distribution over the entire wall plate reached its peak value about 5–10 s after the wall injection initiated and gradually converged to a steady-state value.

References

[1] J.K. Eaton, J.P. Johnston, A review of research on subsonic turbulent flow reattachment, AIAAJ 19 (1981) 1093–1100.
[2] V. de Brederode, P. Bradshaw, Three-dimensional flow in normally two-dimensional separation bubbles: I. Flow behind a rearward-facing step, Aeronautical Report, 72-19, Imperial College, August (1972).
[3] J. Richardson, W.A. de Groot, J.I. Jagoda, R.E. Waiterick, J.E. Hubbartt, E.C. Strahle, Solid fuel ramjet simulators results: experimental and analysis in cold flow, J. Propulsion Power 24 (1985) 1956–1963.
[4] J.T. Yang, B.B. Tsai, G.L. Tsai, Separated-reattaching flow over a backstep with uniform normal mass bleed, J. Fluids Eng. 116 (1994) 29–35.
[5] G.P. Yogesh, B.N. Raghunandan, Flow structure and heat transfer characteristics behind a diaphragm in the presence of a diffusion flame, Int. J. Heat Mass Transfer 32 (1989) 19–28.
[6] R. Zvuloni, Y. Levy, A. Gany, Investigation of a small solid fuel ramjet combustor, J. Propulsion Power 5 (1989) 269–275.
[7] J.-T. Yang, C.-H. Tsai, High temperature heat transfer of separated flow over a sudden-expansion with base mass injection, Int. J. Heat Mass Transfer 39 (1996) 2293–2301.
[8] J.T. Yang, Y.Y. Wu, S.J. Din, Ignition transient of a polymethylmethacrylate slab in a sudden-expansion combustor, Combust. Flame 98 (1994) 300–308.
[9] A.R. Martin, C. Saltiel, W. Shyy, Heat transfer enhancement with porous inserts in recirculating flows, J. Heat Transfer 120 (1998) 458–467.
[10] R.W. Pitz, W. Daily, Combustion in a turbulent mixing layer formed at a rearward-facing step, AIAAJ 21 (1983) 1565–1570.